Earth Planets Space, **51**, 1287–1296, 1999

Ground-based millimeter-wave observations of ozone in the upper stratosphere and mesosphere over Tsukuba

Tomoo Nagahama[1], Hideaki Nakane[1], Yasumi Fujinuma[1], Mariko Ninomiya[2], Hideo Ogawa[3], and Yasuo Fukui[3]

[1]*National Institute for Environmental Studies, 16-2 Onogawa, Tsukuba, Ibaraki 305-0053, Japan*
[2]*Global Environmental Forum, 24-18 Inarimae, Tsukuba, Ibaraki 305-0061, Japan*
[3]*Department of Astrophysics, Nagoya University, Nagoya 464-8602, Japan*

(Received November 20, 1998; Revised July 30, 1999; Accepted September 6, 1999)

We present ground-based millimeter-wave observations of the upper stratospheric and mesospheric ozone, conducted at the National Institute for Environmental Studies (NIES) in Tsukuba, Japan (36°N, 140°E). The measurements were started in October 1995. The millimeter-wave radiometer used for the present study is equipped with the superconductor-insulator-superconductor (SIS) mixer receiver and the acousto-optical spectrometer (AOS). Vertical profiles of ozone mixing ratio from 20 to 80 km were retrieved from the observed ozone spectra for 23 months from October 1996 to August 1998 by using the weighted-damped least squares algorithm adopted for differential emission. Vertical resolution is estimated to be 14 km from the averaging kernels. The total random error on the retrieval is estimated to range from 3 to 13% in summer, and from 2 to 9% in winter, respectively, between 38 and 76 km in altitude. The ozone number density at 38 km with the radiometer which was convolved with the vertical resolution of the lidar agrees well with that of the lidar within a systematic difference of 1%, indicating that the millimeter-wave data at 38 km are validated by the lidar measurements. Annual and semi-annual variations are clearly seen at 50 and 76 km, respectively, in the time series of the ozone mixing ratio observed during 23 months. The annual variation at 50 km is consistent with that in the climatological models. The semi-annual variation at 76 km observed in this work is similar to that of the Solar Mesospheric Explorer (SME) data, except that the ozone mixing ratio in spring measured with SME is about 1.7 times larger than that in autumn while those with the radiometer are almost same.

1. Introduction

As a result of countermeasures against destruction of the ozone layer, chlorine loading will have its maximum level around 2000, and then is expected to decrease gradually. Trends of ozone depletion are most significant in the lower stratosphere from 15 to 20 km and in the upper stratosphere near 40 km. Although recovery of the ozone layer in the lower stratosphere is suggested to depend largely on the "other things" such as climate change (e.g., Austin *et al.*, 1992), the ozone layer in the upper stratosphere is expected to recover according to the decrease of the chlorine loading. Ozone monitoring at this altitude range is, therefore, important to provide evidence for the recovery of the ozone layer.

In order to detect the ozone depletion and recovery of the ozone layer, and to understand their processes, vertical distributions of various minor constituents including ozone in the stratosphere have been measured with various ground-based instruments. Among them, a ground-based millimeter-wave radiometer is one of the major ground-based instruments. Lidar is another important ground-based technique and both contribute significantly to global network of observations such as the Network for Detection of Stratospheric Change (NDSC). Many millimeter-wave measurements have been carried out in the past decades; for example, O_3 (e.g. Connor *et al.*, 1987; Zommerfelds *et al.*, 1989; Ricaud *et al.*, 1991; Parrish *et al.*, 1992; Connor *et al.*, 1994; Kawabata *et al.*, 1994; Cheng *et al.*, 1996), ClO (e.g. de Zafra *et al.*, 1987, 1995; Ricaud *et al.*, 1997), and N_2O (e.g. Parrish *et al.*, 1988; Crewell *et al.*, 1995). These measurements have brought us valuable information on chemical and dynamical processes in the stratosphere and mesosphere.

The millimeter-wave measurements use molecular emission lines which are generally due to pure rotation transitions. Therefore, we can measure the emission spectra all the day because they do not require any light sources unlike absorption and scattering measurements. Continuous measurements provide us with information on variations of the vertical distributions of the minor constituents in the middle atmosphere with various timescales. After removing such time variations, we can detect the long-term trend at each altitude. Moreover, spectral intensities at the millimeter wavelength can be accurately calculated in the forward model since molecular line parameters in the millimeter wavelength region are well defined as compared to those in the infrared region. In addition, the millimeter-wave radiation is not affected by aerosols. Therefore, the vertical profile of ozone mixing ratio can be calculated exactly from equations of the radiative transfer at the millimeter wavelength.

In 1988, the National Institute for Environmental Studies (NIES) at Tsukuba, Japan (36°N, 140°E) started observations

of the vertical distribution of ozone from 20 to 40 km with a lidar, and it is one of the complimentary measurements of NDSC. However, it is insufficient in altitude coverage and in observation frequency in order to monitor the ozone depletion due to gas phase reactions near 40 km which is most efficient in the upper stratosphere. To observe ozone distributions at higher altitudes with considerable frequency, we installed a millimeter-wave radiometer in 1995 and have been measuring the vertical distribution from 38 to 76 km.

High resolution spectroscopy is required for retrieving the vertical profile of ozone in the upper stratosphere and mesosphere since a spectrum of the ozone emission from such an altitude shows a narrow line shape due to small air pressure. In addition, the receiver must have high sensitivity in order to obtain a low noise spectrum with such high frequency resolution. For these reasons, our instrument is equipped with a superconductor-insulator-superconductor (SIS) mixer receiver and an acousto-optical spectrometer (AOS). The SIS mixer receiver provides an extremely low noise temperature close to quantum limit, with which we can obtain the ozone spectra with high signal-to-noise ratio in much shorter observing time than previous measurements with the Schottky diode mixer receivers. The AOS has higher frequency resolution than the filter bank spectrometers, which permits more detailed measurements of pressure-broadened line shapes.

For data analysis, we developed a new algorithm based on the optimal estimation algorithm given by Rodgers (1976), which is commonly used for the analysis of millimeter-wave data. Our algorithm is improved not to change the vertical resolution of the retrieved ozone profile for each spectrum having a different noise level. It is also adapted to the retrieval using the finite differentiation data of the spectrum at the two different frequencies, because it is difficult to determine the baseline of the spectrum observed with the frequency switching technique.

In this paper, we briefly describe the instrument, the observation techniques and the calibration method in Section 2. In Section 3, the retrieval procedure and the error analysis are described. The vertical profiles of ozone obtained by using the millimeter-wave instrument as well as a comparison with the co-located ozone lidar results are discussed in Section 4. In Section 5, we summarize the results.

2. Instrument, Observation Techniques and Calibration

The instrument consists of an antenna, a heterodyne receiver and a spectrometer, and is tuned to observe the $6_{1,5}$ to $6_{0,6}$ transition of ozone at 110.836 GHz. This is basically the same system employed in Nagoya University (Kawabata *et al.*, 1994). The block diagram of the instrument is shown in Fig. 1. The millimeter-wave radiation from the atmospheric ozone is collected by the offset parabolic antenna with a 10 cm diameter whose beam size is 1.8°. The axis of the antenna is pointed toward the north-east at an elevation angle of 45° during observation and toward the hot reference during calibration. The temperature of the hot reference is 300 K which is chosen because it was close to the ambient room temperature. The collected radiation is detected by the 4 K-cooled SIS mixer receiver whose noise temperature is 50 K in single side band (SSB). The SIS mixer receiver is operated in SSB

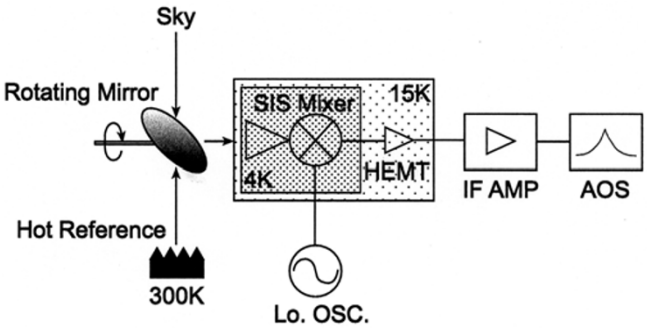

Fig. 1. Block diagram of the millimeter wave radiometer in NIES.

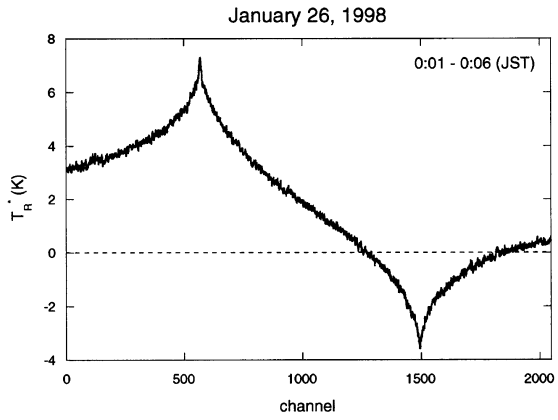

Fig. 2. Millimeter-wave emission spectrum of ozone obtained by using the frequency switching method.

mode by tuning it, and the response of the image side band is suppressed by 13 dB or less than that of the signal side band. The AOS is equipped with 2048 channels, which covers a 60 MHz bandwidth with a 40 kHz frequency resolution. The whole system is operated continuously under the control of a PC-type microcomputer.

Spectral data were obtained by using the frequency switching technique in order to eliminate the background continuum of the spectrum. The central observing frequencies differing by Δf are switched every 2 seconds, and the brightness temperature measured at the frequency f_i, $T(f_i)$, is subtracted to that at $f_i + \Delta f$, $T(f_i + \Delta f)$, where i is the channel number of AOS. The result $\Delta T(f_i) \equiv T(f_i) - T(f_i + \Delta f)$ was averaged during 5 minutes and was stored as the spectral data. Here, we used $\Delta f = 30$ MHz. Figure 2 shows an example of the millimeter-wave emission spectrum of ozone. The ozone spectrum used for analysis was obtained by averaging the two spectra of $\Delta T(f_i)$ and $-\Delta T(f_i - \Delta f)$ because those are the same signal of ozone. Due to this process, the spectral signal-to-noise ratio is improved by a factor of $\sqrt{2}$ because the two signals are independent. This is the advantage of using the frequency switching technique. Typical root-mean-square (rms) noise temperatures of the ozone spectra were 0.07 K in winter and 0.15 K in summer.

Observed spectral intensities must be corrected for absorption in the troposphere and be calibrated by using calibration standards. We used the chopper wheel method for correction

and calibration, in which two sources of thermal emission from the hot reference and the sky, respectively, are used as calibration standards. We measured the radiation from the two calibration sources by rotating the antenna before each ozone measurement was made. Since the Rayleigh-Jeans approximation to the Plank radiation law is valid in the millimeter-wave region, the brightness temperature is proportional to the received intensity. Therefore, the intensities from the sky and the hot reference, I_{sky}, I_{ref}, are expressed as follows,

$$I_{sky} = \alpha \cdot [T_{sky} \cdot (1 - \exp(-\tau_{trop})) + T_{sys}], \quad (1)$$

$$I_{ref} = \alpha \cdot (T_{ref} + T_{sys}), \quad (2)$$

where α is the proportional constant, T_{sky} and T_{ref} the brightness temperatures of the sky and hot reference, respectively, T_{sys} the system temperature and τ_{trop} the optical depth of the tropospheric absorbing layer which is the tropospheric opacity integrated over the line-of-sight. The intensity including the ozone emission from the sky, I_{ozone}, is also expressed by,

$$I_{ozone} = \alpha \cdot [T_{ozone} \cdot \exp(-\tau_{trop}) + T_{sky} \cdot (1 - \exp(-\tau_{trop}) + T_{sys}], \quad (3)$$

where T_{ozone} is the brightness temperature of the ozone emission. Assuming $T_{sky} = T_{ref}$, T_{ozone} is derived from the above equations as follows,

$$T_{ozone} = T_{ref} \cdot (I_{ozone} - I_{sky})/(I_{ref} - I_{sky}). \quad (4)$$

Equation (4) includes no calibration constant and no correction term for the tropospheric absorption. However, we should note that the assumption, $T_{sky} = T_{ref}$, causes errors in calibration while it is not large. Errors including this calibration error are discussed in the following section. Also it should be noted that to measure I_{sky} is difficult because we cannot eliminate the ozone emission toward the sky. To avoid this difficulty, we used I_{ozone} integrated during a very short time of 4 seconds as I_{sky} in the present study. Because the sky emission is typically by one order of magnitude larger than that of the ozone emission, we can assume that the ozone emission is still confused in the short time integrated I_{ozone} and is negligible. In practice, although this assumption causes a systematic error on the spectral intensity, the error was estimated to be negligible.

The millimeter-wave observations have been carried out since October 1995. Because the image side band response of the receiver had not been suppressed sufficiently until September 1996, accuracy of the brightness temperature of the spectrum was worse than that of the later observations. Therefore, we need further corrections to use those data. After tuning the receiver to the SSB mode in October 1996, the brightness temperature of the spectrum became accurate. For this reason, we only used the spectra obtained since October 1996 in the present analysis.

3. Analysis

3.1 Forward model and retrieval

As mentioned above, under the Rayleigh-Jeans approximation, the intensity of the observed spectrum is expressed in the brightness temperature. The brightness temperature of the ozone emission $T_B(f_i)$ is calculated from the equation of radiative transfer, which is integrated over the altitude range as follows,

$$T_B(f_i) = \int_0^\infty K_i(T, n, z, \theta) \cdot R(z) \cdot \sec\theta \cdot dz, \quad (5)$$

where $K_i(T, n, z, \theta)$ is the weighting function at the frequency f_i, θ the zenith angle during observations and $R(z)$ the ozone mixing ratio at the altitude z. The weighting function is the product of temperature T, air density n, absorption coefficient of ozone κ, and optical depth toward the zenith, $\tau_0 \equiv -\int \kappa dz$ (see Parrish *et al.*, 1992), given by,

$$K_i(T, n, z, \theta) = T(z) \cdot n(z) \cdot \kappa(T, f_i) \cdot \exp(-\tau_0 \cdot \sec\theta). \quad (6)$$

We computed the weighting function by adopting models of the vertical profiles of temperature and pressure at 36°N which were obtained by using linear interpolation from the CIRA1986 climatology (Rees *et al.*, 1990) at 35°N and 40°N. For calculation of the absorption coefficient, molecular line parameters were taken from the HITRAN96 database (Data are archived in CD-ROM by Rothman, 1996). And we also used the Voigt symmetrical line profile as a line shape of ozone emission.

In the frequency switching observations, we cannot determine $T_B(f_i)$ itself because the ozone emission at the lower altitude as well as the background continuum including the system noise are eliminated. Therefore, we used a finite differentiation of the brightness temperature at the two different frequencies $\Delta T_B(i) \equiv T_B(f_{i+1}) - T_B(f_i)$, instead of $T_B(f_i)$. The observed spectra were fitted by the third order spline to decrease the error due to noise in making $\Delta T_B(i)$. The equation of radiative transfer for $\Delta T_B(i)$ is expressed in the form,

$$\Delta T_B(i) = \int_0^\infty W_i(T, n, z, \theta) \cdot R(z) \cdot \sec\theta \cdot dz, \quad (7)$$

where $W_i(T, n, z, \theta)$ is the weighting function for differential emission defined as follows,

$$W_i(T, n, z, \theta) \equiv K_{i+1}(T, n, z, \theta) - K_i(T, n, z, \theta). \quad (8)$$

We note that $W_i(T, n, z, \theta)$ is nearly a diagonal matrix, and therefore, $\Delta T_B(i)$ is almost proportional to $R(z)$ at the altitude of z where $W_i(T, n, z, \theta)$ has a maximum value.

The ozone mixing ratio was retrieved from the observed spectrum by using the weighted-damped least squares solution (e.g. Menke, 1989) which is a general form of the optimal estimation algorithm (Rodgers, 1976). It is known that the vertical resolution is improved as the spectral signal-to-noise ratio improves in retrieval processes (Connor *et al.*, 1995). In the optimal estimation algorithm, the vertical resolution depends on adjustable parameters such as noise of the spectrum. These parameters are generally determined to optimize the vertical resolution for each spectrum. In practice, the vertical resolutions in summer tend to be worse than those in winter since spectral rms noise temperatures in summer are typically larger than those in winter. However, it is highly required for monitoring the long-term trends of ozone that the vertical resolution is constant. To avoid the change in

vertical resolution according to the spectral signal-to-noise ratio, we fixed these adjustable parameters in this work. Using the optimal estimation algorithm (Rodgers, 1976), the retrieved vertical profile of ozone mixing ratio R_{est} is given by,

$$R_{est} = R_{init} + S_R W^T (W S_R W^T + S_e)^{-1} (\Delta T_B - W R_{init}), \tag{9}$$

where R_{init} is the a priori vertical profile of ozone mixing ratio, S_R and S_e are the covariances of the a priori vertical profiles of ozone and the spectral measurements, respectively, W the weighting function for differential emission.

In the present study, because S_R has no correlation with the altitude and is treated as an adjustable parameter to optimize the vertical resolution, we put $S_R = \zeta^2 U$ in Eq. (9), where U is an unit matrix, ζ is the proportional constant. For S_e, because the rms noise temperature at each channel is expected to be the same and there is no significant channel-to-channel correlation in the spectrum, we also put $S_e = \epsilon^2 U$, where ϵ is the proportional constant. Eq. (9) is, therefore, derived as,

$$R_{est} = R_{init} + W^T [W W^T + (\epsilon/\zeta)^2]^{-1} (\Delta T_B - W R_{init}), \tag{10}$$

where $(\epsilon/\zeta)^2$ is the adjustable parameter to optimize the vertical resolution. If we adopt small $(\epsilon/\zeta)^2$, the vertical resolution become high, but the error on the retrieval which causes an oscillation in the retrieved profile increases. We empirically determined $(\epsilon/\zeta)^2 = 0.01$ in order to give vertical resolution as high as possible without ambiguous oscillations in the retrieved vertical profile of ozone by using the typical spectrum in summer. In this case, the random error on the retrieval is within 13% for measurements in summer.

Daily a priori profiles of ozone mixing ratio R_{init} were constructed by the following procedure. First, we made daily vertical profiles of ozone mixing ratio with the spline interpolation of monthly mean ozone profiles which are obtained from the ozonesonde data for the altitudes below 25 km at Tateno (36°N, 140°E) in 1994 and 1995 (Data are archived in CD-ROM by World Ozone and Ultraviolet radiation Data Center (WOUDC), Vol. 1 August 1996) and the model above 35 km at 36°N given by Keating *et al.* (1990). These were used as R_{init} for making further realistic a priori profiles of ozone since these do not include the diurnal variation which is evident in the mesosphere. Tentative vertical profiles were retrieved from the ozone spectra observed in 1997. Using the tentative profiles obtained from 9 a.m. to 3 p.m. and from 9 p.m. to 3 a.m. in local time, we calculated monthly means in the daytime and nighttime. Finally, daily vertical profiles in the daytime and nighttime which we use as R_{init} in actual retrieval were reconstructed with the spline interpolation of the daytime and nighttime monthly means, respectively, in time.

Figure 3 shows examples of averaging kernels A which are expressed as

$$A = W^T [W W^T + (\epsilon/\zeta)^2]^{-1} W. \tag{11}$$

The vertical resolution was defined as a full width at half maximum (FWHM) of the averaging kernel for each altitude, and was estimated as 14 km between 38 to 76 km in altitude.

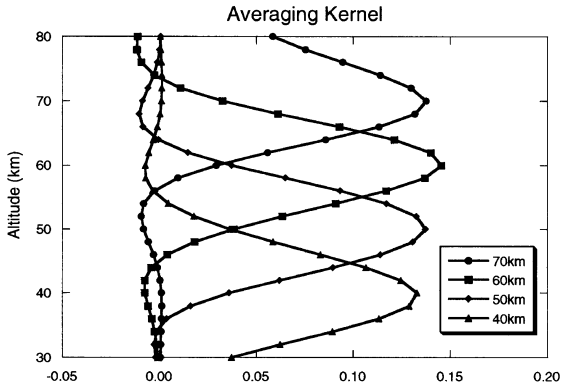

Fig. 3. Examples of averaging kernels, which were calculated for every 2 km from 38 to 76 km.

3.2 Error analysis

Here we evaluate influence of systematic and random errors on the retrieved vertical profiles of ozone mixing ratio. In the present study, accuracy and precision appearing on the retrieved ozone profile rather than those of error sources themselves were treated as the systematic and random errors, respectively. The systematic errors are mainly caused by (1) the chopper wheel calibration method, (2) incomplete suppression of the image side band response of the receiver, and (3) uncertainty of molecular line parameters. The errors due to the former two sources can be corrected for by using the instrument parameters and the climatological data, while it is difficult to correct for the latter one. The random errors are mainly due to (1) difference in temperature profiles, (2) difference in a priori vertical profile of ozone, and (3) random noise on the spectrum. In the following subsection, we evaluated these errors in order.

3.2.1 Systematic error First of all, we estimated the error due to the chopper wheel calibration method itself. In this method, thermal radiation from the hot reference and the sky are used as calibration standards. Although the temperature of the hot reference is stable at 300 K, the effective sky temperature strongly depends on the tropospheric opacity which is mainly determined by the amount of water vapor in the troposphere toward the line-of-sight because it is close to the temperature at the altitude where the ozone emission from the stratosphere is most absorbed. The effective sky temperature at 110 GHz was roughly estimated as the temperature in the lower troposphere at 1–2 km (Kawabata *et al.*, 1994), and was also estimated empirically to be ~7 K less than the surface (Parrish *et al.*, 1988). However, in the chopper wheel calibration method, the effective sky temperature is assumed to be equal to that of the hot reference, and the ozone emission is to be negligible compared to that of the sky. These assumptions induce the error in the spectral intensity due to variations of the effective sky temperature and the tropospheric absorption. If the tropospheric absorption is small enough, the error in the spectral intensity is estimated as $\sim \Delta T \tau_{trop}/300$, where ΔT is the difference between the effective sky temperature and 300 K, and τ_{trop} is the optical depth in the troposphere. If we consider seasonal variation of the effective sky temperature, ΔT can be expressed as $\Delta T \equiv \Delta T_{ave} + T_{err}$, where ΔT_{ave} is the dif-

ference the monthly mean of the effective sky temperature and 300 K, and T_{err} is the difference between the actual and the monthly mean. The error in the spectral intensity is, therefore, expressed as $\sim \Delta T_{ave}\tau_{trop}/300 + T_{err}\tau_{trop}/300$. The first and second terms stand for the systematic and random errors, respectively. Using the climatological data at Tsukuba and empirical relationship between the surface and the effective sky temperatures given by Parrish *et al.* (1988), typical ΔT_{ave} was estimated as ~10 K in summer and ~30 K in winter, respectively, and T_{err} was within 3 K. Although it is difficult to know the realistic τ_{trop} at 110 GHz due to lack of climatological data, we can roughly estimate τ_{trop} from the noise level of the observed spectrum, T_{rms}. Using the receive noise temperature, T_{rec}, and the sky temperature, T_{sky}, τ_{trop} is obtained by

$$\tau_{trop} = \ln\left(\frac{\sqrt{tB/2}T_{rms} + T_{sky}}{T_{rec} + T_{sky}}\right), \qquad (12)$$

where t is the integration time and B is the frequency resolution. When we adopted $t = 300$ seconds, $B = 40$ kHz, $T_{rec} = 50$ K, $T_{rms} = 0.15$ K and $T_{sky} = 290$ K in summer, $T_{rms} = 0.07$ K and $T_{sky} = 270$ K in winter, τ_{trop} were estimated as ~0.7 and ~0.3 in summer and winter, respectively. Using ΔT_{ave}, T_{err}, and τ_{trop}, the systematic error caused by the chopper wheel method was estimated to be 2–3% negative in the spectral intensity, and the random error was within 1%. These results indicate that we should consider the systematic error only in the chopper wheel method because the random error is negligible. We note that this systematic error is almost constant in all seasons while ΔT_{ave} and τ_{trop} vary. That is because ΔT is roughly inversely proportional to τ_{trop}, and therefore, a product of ΔT and τ_{trop} is almost constant. Since ΔT is close to the temperature at the most absorbing altitude, if τ_{trop} increases, the altitude decreases, and consequently, ΔT becomes decreasing.

Additional systematic error on the spectral intensity is due to incomplete suppression of the image side band response of the receiver. Our receiver has suppression of 13 dB or less, which causes the systematic error of at most 5% negative on the spectral intensity.

Combining the errors shown above, the systematic error on the spectral intensity was estimated to be 7–8% negative. Using this estimation, the systematic error on the retrieval can be estimated numerically as follows: First, we created a spectrum whose intensity decreased by 8% from the spectrum calculated from the a priori profile of ozone. Then, we retrieved a vertical profile of ozone from this spectrum, and calculated the resulting error. Figure 4 shows the systematic error on the retrieval due to the error on the spectral intensity of 8%, which was estimated to be 6–9% negative ranging from 38 to 76 km in altitude. It should be noted that this systematic error shows little variation due to the sky condition. Therefore, we can make corrections in retrieved results by using this estimation.

The error on the retrieval due to uncertainty in the molecular line parameters was estimated as at most 7% by Connor *et al.* (1994). We used this value in the literature for the error estimation because such a error is independent of the instruments and site conditions. We note that it is difficult to correct for this error since we do not know the practical value of the error without making a detailed comparison with other independent measurements.

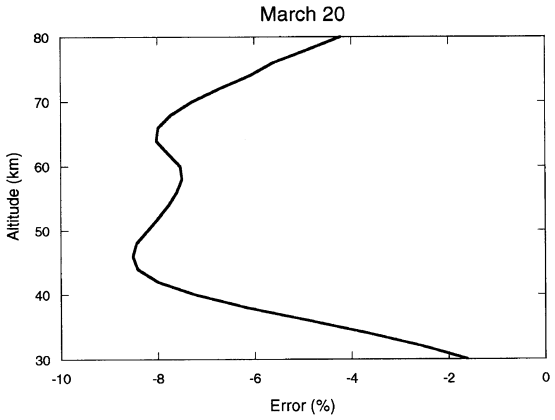

Fig. 4. Estimated systematic error on the retrieval due to the error on the spectral intensity of 8%.

3.2.2 Random error Next, we considered influence of the random errors. As shown above, one of these errors is due to difference in the vertical profile of temperature inputting to the forward model. If the temperature profile we used is different from the actual, the difference causes an error on the retrieval. In the present study, we used the vertical profiles of temperature derived from the CIRA1986 climatology. From the lidar observations of temperature profile over Tsukuba (Nakane *et al.*, 1992), the difference between the observed and climatological temperatures was estimated to be typically within 20%, corresponding to ~40 K, between 30 and 80 km. To assess the influence of such a difference, temperature dependence was estimated numerically by using two virtual profiles of temperature. One is generated by adding a constant error of 40 K to the climatological temperature as inputs to the forward model (Case A), and the other is by adding a constant of 10 K and a random of 30 K (Case B). Figure 5 shows the errors on the retrieval due to the temperature difference in the two cases. The error in Case A was estimated to be within 6% up to 60 km and 8% at 70 km, and that in Case B was within 5%. Considering temperature variations observed by Nakane *et al.* (1992), Case B is more realistic than Case A. Hence, we used Case B as the error due to the temperature profile in the present study. We noted that the error on the retrieval is much smaller than that of temperature because temperature dependence of the observed ozone line is small.

The error due to difference in the a priori profile of ozone was estimated. It is well known that difference between the a priori and actual profiles of ozone results in the error on the retrieval when we calculate the vertical profile of ozone by using inversion methods such as the optimal estimation algorithm (Rodgers, 1990). Here, we considered the deviation of the ozone mixing ratio in the nighttime from their monthly mean as the errors in the a priori profile of ozone in the daytime and nighttime, and also considered the diurnal variation as that in the morning and evening. Because we used the respective a priori profiles for the data in the daytime and nighttime, the deviation from the monthly mean can be used as a typical error in the a priori profile of ozone. In contrast,

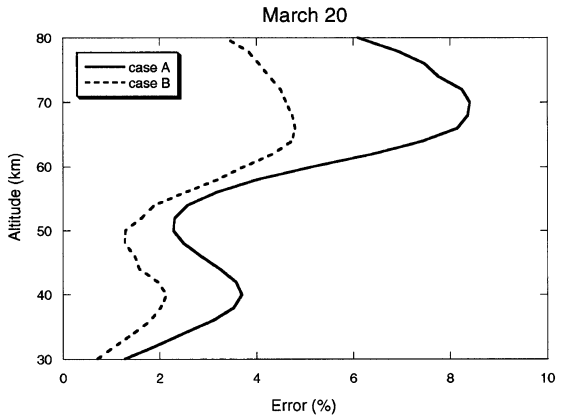

Fig. 5. Estimated random errors on the retrieval due to the temperature differences in two cases. Case A: 40 K constant error (solid). Case B: 10 K constant and 30 K random errors (dashes).

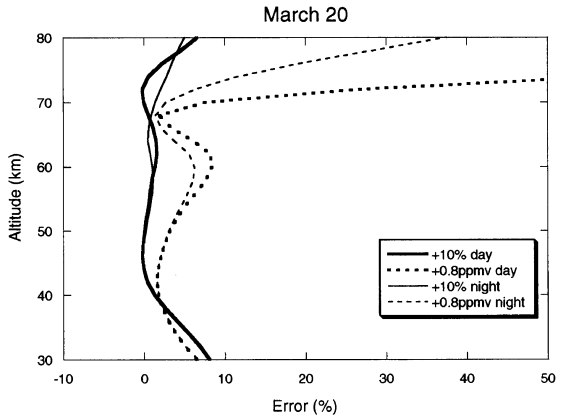

Fig. 6. Estimated random error on the retrieval due to errors in the a priori profiles of ozone. Solid lines are the cases that the errors are 10% larger than the a priori ozone values. Dashed lines indicate the cases of a constant error of 0.8 ppmv. The errors in the daytime and nighttime are presented by thick and thin lines, respectively.

for the data in the morning and evening, we used the a priori profile in the daytime for retrieval at present. In this case, the difference between the a priori and the actual profiles of ozone is at most as same as an amplitude of the diurnal variation. If we adopt the a priori profile interpolated those in the daytime and nighttime according to the observed time, the difference becomes much smaller than that estimated above. According to Connor *et al.* (1994), the deviation of ozone mixing ratio observed in the nighttime from the monthly mean was estimated to be less than 7%, and the diurnal variation was within ∼0.8 ppmv below 0.04 mPa corresponding to ∼70 km in altitude. To estimate influence of this error, we made four different vertical profiles of ozone as inputs to the retrieval. The two profiles were generated by adding 10% values of ozone mixing ratio to the a priori profiles of ozone in the daytime and nighttime on March 20, respectively, which stand for typical a priori profiles in the daytime and nighttime. The rest of the profiles were also made by adding 0.8 ppmv to the a priori profiles in the daytime and nighttime, respectively, standing for those in the morning and evening. Using these profiles, error dependence on the a priori profiles of ozone was estimated numerically with the same manner as that on the vertical profile of temperature. The errors on the retrieval are shown in Fig. 6. In the former two cases, the errors on the retrieval were estimated to be within 3% from 38 to 76 km, and those in the latter cases were within 10% below 70 km in the daytime and 74 km in the nighttime, respectively.

The random noise on the spectrum is an important source of the random errors on the retrieval. We also estimated this error numerically with the same manner shown above by using two spectra made by adding the random noise of 0.15 K and 0.07 K which were typical values in summer and winter, respectively, to a spectrum calculated by the forward model. Figure 7 shows the errors on the retrieval. In the summer case, the error ranged from 2 to 12% between 38 and 76 km, and increased rapidly above 56 km. The error in winter was within 7%, which is generally smaller than that in summer.

The total of the random errors on the retrieval can be expressed by root sum square of each error, if we assume that

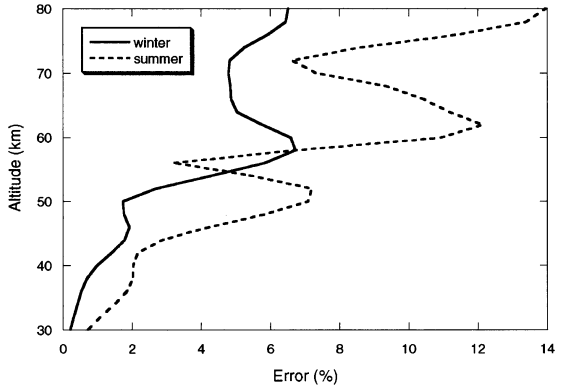

Fig. 7. Estimated random errors on the retrieval due to random noises on the spectrum in winter (solid) and summer (dashes), respectively.

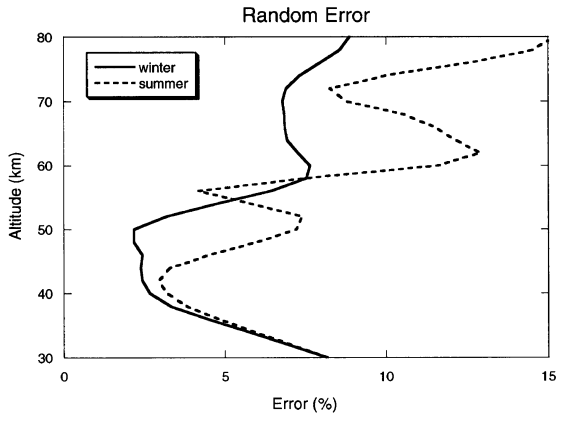

Fig. 8. Total of the random errors on the retrieval in winter (solid) and summer (dashes), respectively.

they are independent of each other. In Fig. 8, we demonstrate the totals of the random errors in summer and winter, respectively. They ranged from 3 to 13% in summer, and from 2 to 9% in winter, respectively, between 38 and 76 km

in altitude.

4. Results and Discussion

The ozone spectrum was made from the observed spectrum such as shown in Fig. 2 by averaging the two spectra which were observed and shifted itself by −30 MHz. In Fig. 9, we show the ozone spectra averaged for one hour in the daytime and nighttime obtained on January 26, 1998 with residuals of fitting by the forward model calculation. The vertical profiles of ozone mixing ratio retrieved from those spectra are shown in Fig. 10. The intensity near the line center of the spectrum in the nighttime is much stronger than that in the daytime, as shown in Fig. 9. This feature is reflected in enhancement of the mesospheric ozone in the nighttime which is one of the important features of ozone distributions in the mesosphere (e.g. Zommerfelds *et al.*, 1989). We confirmed by this result that the vertical profile of ozone is truly retrieved from the observed spectrum.

4.1 Comparison with lidar measurements

In order to validate the retrieved profiles of ozone, we compared between ozone number densities at 38 km measured with the millimeter-wave radiometer and the ozone lidar in NIES. We used the data obtained from January 1997 to February 1998 when the lidar measurements were carried out. To make the comparison quantitatively, it is necessary to consider the different vertical resolutions of the millimeter-wave radiometer and the lidar, which are 14 km and 5 km, respectively, at 38 km. Thus, we should convolve each vertical profile of ozone with the other vertical resolution to make the comparison with the same resolution. The convolved profile of the lidar measurement x_c was obtained by,

$$x_c = x_a + A \cdot (x_l - x_a), \tag{13}$$

where x_a is the a priori profile of ozone density, x_l is the measurement with the lidar and A is the averaging kernel of the radiometer. The averaging kernels were calculated by using monthly means of the temperature, pressure, air density and the a priori profile of ozone mixing ratio. Since x_l has typical altitude coverage up to 42 km which does not cover the full altitude range to compute x_c at 38 km, we extended x_l above 42 km by using the a priori profile of ozone. The convolved profile of the radiometer measurement was also calculated by the same manner except that response for an ozone concentration at 38 km given like δ-function was used as A of the lidar measurements. We note that such a response is exactly the same as the averaging kernel. If we assume $x_l = x_a + \delta$, where δ is the ozone concentration at the altitude, Eq. (13) can be expressed as $x_c = x_a + A\delta$, indicating that A is the response for δ. The response for the ozone concentration at 38 km of the lidar measurement was calculated numerically from the differential absorption lidar (DIAL) equation adopted for the NIES ozone lidar (Nakane *et al.*, 1993). The vertical profiles of ozone as inputs to the DIAL equation were computed from the monthly mean of the a priori profile of ozone density. For the millimeter-wave measurements, the convolved ozone number densities in the daytime and nighttime at 38 km were derived from the observed data averaged for 6 hours from 9 a.m. to 3 p.m. and from 9 p.m. to 3 a.m. of the next day, respectively. The

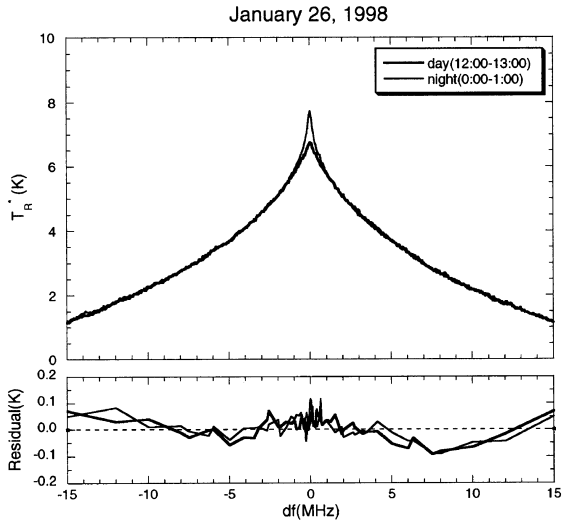

Fig. 9. Observed ozone spectra and their residuals of fitting by the forward model calculation. Thick and thin lines are the spectra averaged in 1 hour of the daytime and nighttime, respectively.

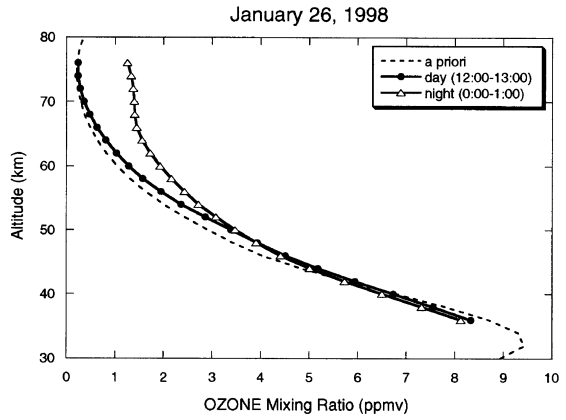

Fig. 10. Vertical profiles of ozone mixing ratio with the a priori profile on January 26, 1998. Solid circles and open triangles indicate the values retrieved from the spectrum averaged in 6 hours of the daytime and nighttime, respectively.

millimeter-wave data were made corrections of the systematic error on the spectrum intensity, which was 6% negative at 38 km.

Time variations of the convolved ozone number densities at 38 km with the radiometer and the lidar are shown in Fig. 11, and a correlation plot of the two measurements is displayed in Fig. 12. It is remarkable that the two measurements agree well within the systematic difference of 1%. The correlation coefficient is 0.77. Such a good agreement indicates that the millimeter-wave data at 38 km are validated by the lidar measurements. The small systematic difference can be understood due to the systematic error of each measurement since the radiometer and lidar measurements have the systematic errors of at most 7% and 10%, respectively (Nakane *et al.*, 1992). Dispersion of the two measurements was estimated to be 7% with the standard deviation. This is mainly due to the random error of the lidar measurements.

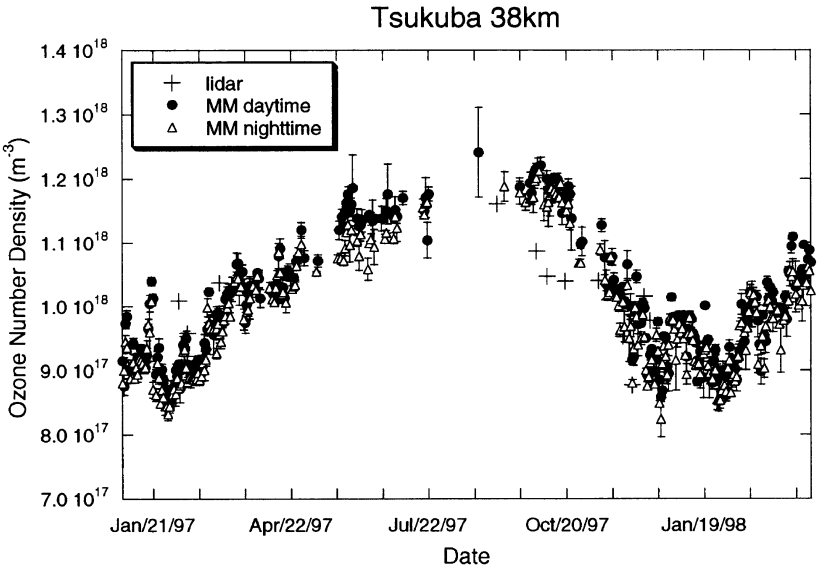

Fig. 11. Ozone number densities at 38 km for the millimeter-wave radiometer and lidar in NIES from January 1997 to March 1998. Solid circles and open triangles denote the 6 hours averaged values with the radiometer in the daytime and nighttime, respectively, and pluses are the lidar values. The error bars show the standard deviation of the scatter of the data over 6 hours. The radiometer and lidar data were convolved by their vertical resolutions.

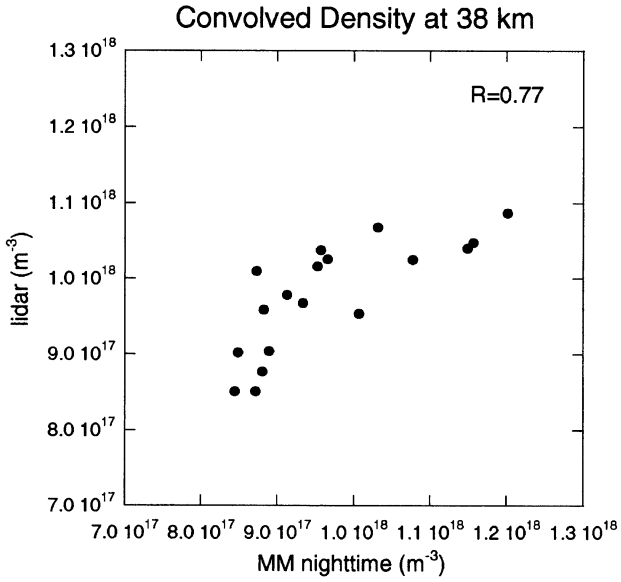

Fig. 12. Correlation between the measurements with the radiometer and lidar in NIES.

In Fig. 11, we can see a large scatter of the lidar measurements compared with those of the radiometer. The random error of the lidar measurements was estimated to be within 10% (Nakane *et al.*, 1992), which is much larger than that of the radiometer within 3%. The dispersion we estimated is consistent with that derived from the error estimation if we consider that the typical value of the random error with the lidar is smaller than that estimated.

4.2 Annual and semi-annual variations of ozone

In Fig. 13, we show radiometer measurements of ozone mixing ratio at 50 and 76 km since October 1996. The daytime and nighttime data were averaged in 6 hours from 9 a.m. to 3 p.m. and from 9 p.m. to 3 a.m. of the next day, respectively. The systematic error on the retrieval at each altitude due to the intensity scale error estimated in the Subsubsection 3.2.1, was corrected. We found in Fig. 13 seasonal and short-term variations of ozone mixing ratio. At 50 km, a remarkable feature is an annual variation that the ozone mixing ratio is minimum in summer and maximum in winter, which is basically consistent with the climatological model at 50°N (Keating *et al.*, 1990). The observed amplitude of the annual variation was estimated as 15% of the annual mean, being close to that of the model. Standard deviation of ozone mixing ratio within each month was typically 5% of the annual mean. Although a semi-annual variation of ozone mixing ratio also seems to be seen at 50 km, because short-term variations are more evident than the semi-annual, we did not distinguish them in this work. To evaluate such a semi-annual variation of ozone, further long-term observations are desired. One of the most evident short-term variations occurred in November 1997, when the ozone mixing ratio increased by about 25% during a few days time and it sustained for a few weeks time at 50 km. This sudden increase of the ozone mixing ratio was accompanied by the temperature decrease of ∼25 K observed with the NIES lidar. In the lower mesosphere, various dynamical effects modulate the temperature, which affects the ozone mixing ratio through the temperature dependence of chemical processes.

The most remarkable feature at 76 km is an apparent semi-annual variation of ozone mixing ratio which is clearly seen in both the plots of the daytime and nighttime data. The present results revealed such a feature more clearly than the previous millimeter-wave data (Kawabata *et al.*, 1997) because the measurements were carried out more frequently and the retrieval algorithm is more accurate than the previous works. Ozone mixing ratio in spring and autumn was 0.3 ppmv in the daytime and 2.3 ppmv in the nighttime, respectively, which is about twice as large as that in summer and winter. A similar semi-annual variation of the ozone mixing

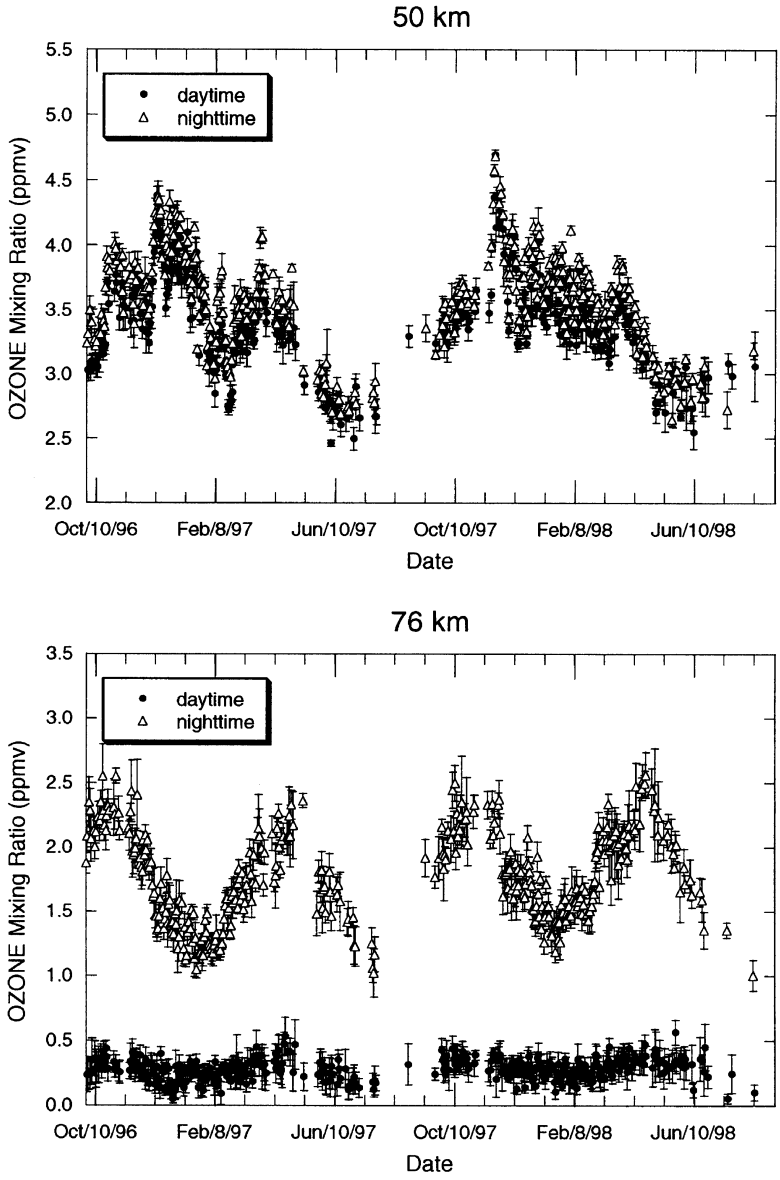

Fig. 13. Variations of ozone mixing ratios at 50 and 76 km from October 1996 to August 1998. Solid circles and open triangles are the values averaged in 6 hours of the daytime and nighttime, respectively. The error bars show the standard deviation of the scatter of the data over 6 hours.

ratio was also seen in the Solar Mesospheric Explorer (SME) data. The semi-annual variation observed in the present study is well fitted by a single sine curve with a half year period, and its amplitude was estimated to be 30% of the annual mean. However, the SME measurements show the variation that the ozone mixing ratio in spring was about 1.7 times larger than that in the autumn (Thomas, 1990). This discrepancy cannot be explained by difference in vertical resolution. The ozone mixing ratios observed with SME at the altitude ranging 70 to 80 km show almost the same semi-annual variation that the ozone mixing ratio in spring is larger than that in the autumn while the spring peak at 80 km is delayed about 2 months from that at 70 km. Therefore, even if we convolve these profiles with the vertical resolution of the radiometer, the convolved ozone mixing ratio should show almost the same feature of variation with SME at 76 km. As a result of least squares fit with annual and semi-annual sine functions and a straight line to the SME data, the amplitude of the semi-annual variation measured with the SME was estimated as 40%, being slight larger than the present result. This may be due to difference in vertical resolution. It might be shown a good agreement with them after we convolve the SME measurement with the vertical resolution of the radiometer, while we cannot convolve it due to lack of information on the vertical resolution and numerical data of the SME in the present work.

As the photochemical lifetime of the Ox family around 76 km is 2–3 hours (Garcia and Solomon, 1985), the semi-annual variation of ozone mixing ratio can be understood by photochemical changes due to influence of some dynamical processes which make semi-annual variation of constituents being important for the photochemistry of ozone. Garcia and Solomon (1985) explained that the semi-annual variation revealed with SME is caused by the gravity-wave-driven diffusion of water vapor from the lower altitude region, which induces the increase of HO_x, and consequently, the ozone

mixing ratio decreases. From the MU radar studies on gravity wave activity, Murayama *et al.* (1994) revealed a semi-annual variation of the gravity wave energy in the upper mesosphere at 65–85 km, that has maxima in summer and winter and minima in spring and autumn. There is no significant difference between the spring and autumn minina, which leads to the result that the ozone mixing ratios in the upper mesosphere are expected to be the same in spring and autumn. One difficulty in understanding the mechanism of the semi-annual variation of ozone is that the water vapor mixing ratio measured in the upper mesosphere shows a predominantly annual variation (Nedoluha *et al.*, 1995). Theories are, therefore, required to explain the new findings of the present study.

5. Conclusion

We have newly installed the millimeter-wave radiometer at Tsukuba, Japan to observe the ozone variations in the upper stratosphere and mesosphere, and have retrieved the vertical profiles of ozone mixing ratio by using the weighted-damped least squares algorithm for a period from October 1996 to August 1998. The main results are summarized as follows:

1. From the error analysis of the measurements, the total random error in the retrieved profile was estimated to be typically within 10% ranging between 38 and 76 km in altitude.

2. The convolved ozone number density at 38 km with the radiometer agrees well with that of the lidar within the systematic difference of 1%. This indicates that the radiometer measurements at 38 km are validated by those of the lidar.

3. From 23 months observations, we clearly detected annual and semi-annual variations of the ozone mixing ratio at 50 and 76 km, respectively. The annual variation at 50 km is consistent well with the climatological models.

4. The semi-annual variation of the ozone mixing ratio at 76 km detected in the present work is similar to the SME data except that the ozone mixing ratio in spring measured with SME is about 1.7 times larger than that in autumn while those with the radiometer are almost the same.

Acknowledgments. The authors thank to M. Suzuki and A. Morihira of Fujitsu VLSI Ltd. for the maintenance of the millimeter-wave instrument. We also thank P. S. Namboothiri of NIES and G. E. Nedoluha of Naval Research Laboratory for careful reading of the manuscript and valuable comments. This work is one of the projects of the Global Environment Monitoring of the Center for Global Environment Research (CGER) in NIES. T. Nagahama gratefully acknowledges support from a Domestic Research Fellowship of Japan Science and Technology Corporation (JST).

References

Austin, J., N. Butchart, and K. P. Shine, Possibility of an Arctic ozone hole in a doubled-CO2 climate, *Nature*, **360**, 221–225, 1992.

Cheng, D., R. L. de Zafra, and C. Trimble, Millimeter wave spectroscopic measurements over the South Pole, 2. An 11-month cycle of stratospheric ozone observations during 1993–1994, *J. Geophys. Res.*, **101**, 6781–6793, 1996.

Connor, B. J., J. W. Barrett, A. Parrish, P. M. Solomon, R. L. de Zafra, and M. Jaramillo, Ozone over McMurdo Station, Antarctica, austral spring 1986: Altitude profiles for the middle and upper stratosphere, *J. Geophys. Res.*, **92**, 13221–13230, 1987.

Connor, B. J., D. E. Siskind, J. J. Tsou, A. Parrish, and E. E. Remsberg, Ground-based microwave observations of ozone in the upper stratosphere and mesosphere, *J. Geophys. Res.*, **99**, 16757–16770, 1994.

Connor, B. J., A. Parrish, J. J. Tsou, and M. P. McCormick, Error analysis for the ground-based microwave ozone measurements during STOIC, *J. Geophys. Res.*, **100**, 9283–9291, 1995.

Crewell, S., D. Cheng, R. L. de Zafra, and C. Trimble, Millimeter wave spectroscopic measurements over the South Pole, 1. A study of stratospheric dynamics using N_2O observations, *J. Geophys. Res.*, **100**, 20839–20844, 1995.

de Zafra, R. L., M. Jaramillo, A. Parrish, P. M. Solomon, B. Connor, and J. W. Barrett, High concentrations of chlorine monoxide at low altitudes in the Antarctic spring stratosphere: Diurnal variation, *Nature*, **328**, 408–411, 1987.

de Zafra, R. L., J. M. Reeves, and D. T. Shindell, Chlorine monoxide in the Antarctic spring vortex, 1. Evolution of midday vertical profiles over McMurdo Station, 1993, *J. Geophys. Res.*, **100**, 13999–14007, 1995.

Garcia, R. R. and S. Solomon, The effect of breaking gravity waves on the dynamics and chemical composition of the mesosphere and lower thermosphere, *J. Geophys. Res.*, **90**, 3850–3868, 1985.

Kawabata, K., H. Ogawa, and Y. Yonekura, Ground-based millimeter-wave measurements of mesospheric and stratospheric ozone employing an SIS mixer receiver, *J. Geomag. Geoelectr.*, **46**, 755–770, 1994.

Kawabata, K., H. Ogawa, Y. Yonekura, H. Suzuki, M. Suzuki, Y. Iwasaka, T. Shibata, and T. Sakai, Ground-based radiometry of stratomesospheric ozone employing a superconductive receiver, *J. Geophys. Res.*, **102**, 1371–1377, 1997.

Keating, G. M., M. C. Pitts, and D. F. Young, Ozone reference models for the middle atmosphere, *Adv. Space Res.*, **10**(12), 317–355, 1990.

Menke, W., *Geophysical Data Analysis: Discrete Inverse Theory, Revised Edition*, 289 pp., Academic Press Inc., San Diego, 1989.

Murayama, Y., T. Tsuda, and S. Fukao, Seasonal variation of gravity wave activity in the lower stratosphere observed with the MU radar, *J. Geophys. Res.*, **99**, 23057–23069, 1994.

Nakane, H., S. Hayashida, Y. Sasano, N. Sugimoto, I. Matsui, and A. Minato, Vertical profiles of temperature and ozone observed during DYANA campaign with the NIES ozone lidar system at Tsukuba, *J. Geomag. Geoelectr.*, **44**, 1071–1083, 1992.

Nakane, H, S. Hayashida, N. Sugimoto, I. Matsui, and Y. Sasano, Ozone Lidar Monitoring, *Annual Report on Global Environmental Monitoring (1993)*, Center for Global Environmental Research, National Institute for Environmental Studies, 1–31, 1993.

Nedoluha, G. E., R. M. Bevilacqua, R. M. Gomez, D. L. Thacker, W. B. Waltman, and T. A. Pauls, Ground-based measurements of water vapor in the middle atmosphere, *J. Geophys. Res.*, **100**, 2927–2939, 1995.

Parrish, A., R. L. de Zafra, P. M. Solomon, and J. W. Barrett, A ground-based technique for millimeter wave spectroscopic observations of stratospheric trace constituents, *Radio Sci.*, **23**, 106–118, 1988.

Parrish, A., B. J. Connor, J. J. Tsou, I. S. McDermid, and W. P. Chu, Ground-based microwave monitoring of stratospheric ozone, *J. Geophys. Res.*, **97**, 2541–2546, 1992.

Rees, D., J. J. Barnett, and K. Labitzke, COSPAR International Reference Atmosphere: 1986, Part II: Middle atmosphere models, *Adv. Space Res.*, **12**(12), 1990.

Ricaud, P., J. Brillet, J. de La Noë, and J. P. Parisot, Diurnal and seasonal variations of stratospheric ozone: Analysis of ground-based microwave measurements in Bordeaux, France, *J. Geophys. Res.*, **96**, 18617–18629, 1991.

Ricaud, P., J. de La Noë, R. Lauqué, and A. Parrish, Analysis of stratospheric chlorine monoxide measurements recorded by a ground-based radiometer located at the Plateau de Bure, France, *J. Geophys. Res.*, **102**, 1423–1439, 1997.

Rodgers, C. D., Retrieval of atmospheric temperature and composition from remote measurements of thermal radiation, *Rev. Geophys.*, **14**, 609–624, 1976.

Rodgers, C. D., Characterization and error analysis of profiles retrieved from remote sounding measurements, *J. Geophys. Res.*, **95**, 5587–5595, 1990.

Thomas, R. J., Seasonal ozone variations in the upper mesosphere, *J. Geophys. Res.*, **95**, 7395–7401, 1990.

Zommerfelds, W. C., K. F. Kunzi, M. E. Summers, R. M. Bevilacqua, D. F. Strobel, M. Allen, and W. J. Sawchuck, Diurnal variations of mesospheric ozone obtained by ground-based microwave radiometry, *J. Geophys. Res.*, **94**, 12819–12832, 1989.

T. Nagahama (e-mail: nagahama.tomoo@nies.go.jp), H. Nakane (e-mail: nakane@nies.go.jp), Y. Fujinuma, M. Ninomiya, H. Ogawa, and Y. Fukui